Computational Modeling of Cathodic Limitations on Localized Corrosion of Wetted SS 316L at Room Temperature

MOL.20051117.0248

Fushuang Cui, Francisco J. Presuel-Moreno, Robert G. Kelly

University of Virginia, Department of Materials Science and Engineering

116 Engineer's Way, P.O. Box 400745, Charlottesville, VA 22903

ABSTRACT

The ability of a SS316L surface wetted with a thin electrolyte layer to serve as an effective cathode for an active localized corrosion site was studied computationally. The dependence of the total net cathodic current, I_{net}, supplied at the repassivation potential E_{rp} (of the anodic crevice) on relevant physical parameters including water layer thickness (WL), chloride concentration ($[Cl^-]$) and length of cathode (Lc) were investigated using a three-level, full factorial design. The effects of kinetic parameters including the exchange current density ($i_{o,c}$) and Tafel slope (β_c) of oxygen reduction, the anodic passive current density (i_p) (on the cathodic surface), and E_{rp} were studied as well using three-level full factorial designs of $[Cl^-]$ and Lc with a fixed WL of 25μm. The study found that all the three parameters WL, $[Cl^-]$ and Lc as well as the interactions of Lc x WL and Lc x $[Cl^-]$ had significant impact on I_{net}. A five-factor regression equation was obtained which fits the computation results reasonably well, but demonstrated that interactions are more complicated than can be explained with a simple linear model. Significant effects on I_{net} were found upon varying either $i_{o,c}$, β_c, or E_{rp}, whereas i_p in the studied range was found to have little impact. It was observed that I_{net} asymptotically

approached maximum values (I_{max}) when Lc increased to critical minimum values. I_{max} can be used to determine the stability of coupled localized corrosion and the critical Lc provides important information for experimental design and corrosion protection.

INTRODUCTION

Metal surfaces exposed to moist air form thin layers of water which contain ionic species. These species can originate from the water source (e.g., rain), dissolution of gases or soluble species in any solids present, or from the deliquescence of hygroscopic salts [1,2]. Many materials are passive under atmospheric conditions and are thus susceptible to localized corrosion. Pitting corrosion may initiate on a free surface if the potential is sufficiently oxidizing and the chloride concentration is high [3,4]. Precipitates, metal oxide scales as well as geometrical crevices can generate occluded local geometries that trap electrolytes and thus promote localized corrosion such as crevice corrosion [5]. In both pitting and crevice corrosion, rather than a potentiostat as in most laboratory studies [6,7], it is the external cathode (*i.e.*, the wetted metal surface surrounding the localized corrosion site) that supplies the required cathodic current to maintain the stability of the localized corrosion site. The stability of such a localized corrosion site thus depends on the characteristics of the cathode, including the water layer chemistry (i.e., ionic species and concentration), geometry, temperature, and the electrochemical reaction kinetics (reversible potential $E_{o,c}$, and exchange current density $i_{o,c}$, Tafel slopes β_c, etc). For a wetted cathode linked to an active localized corrosion site, the resistance of the electrolyte between them further complicates the problem as it varies with position on the cathode. The interactions among these factors are complex, and therefore they are

difficult to control and understand based solely on experiments. In addition, the effects of these parameters add significantly to the dimensionality to the problem.

Whereas a systematic experimental study of all these factors is time- and resources-consuming and rather impractical, computational studies can be efficiently performed and can enhance our understanding of this important issue. In addition, although graphical analysis using E-log i plots together with Mixed Potential Theory can qualitatively predict the effects of the electrochemical parameters (i.e. $i_{o,c}$ and β_c), only computational studies can provide quantitative predictions of these effects due to the intervening and distributed resistance of the electrolyte. That said, computations that are disjointed from experimental data are of little use for practical applications. Experimental kinetic data for the relevant electrochemical reactions as well as physiochemical data such as conductivity and diffusion coefficient of oxygen are needed to ground the computations in reality.

To isolate the effects of variables on the ability of wetted metal surface systems to support localized corrosion, one can computationally separate the external wetted surface (cathode) and the crevice (anode), and then model them individually, linking them through the imposition of a common fixed potential at the junction point (i.e., the mouth of the crevice). In the present study, which focused on the external wetted surface, the potential of interest was the repassivation potential of the anodic crevice as this represents the critical point for stability [8,9]. If the projected cathodic current provided by the cathode is smaller than the projected anodic current required by the anode, the localized corrosion cannot stabilize. Computational studies of the anode are ongoing and will be reported in the future.

A limitation to the adaptation of the considerable amount of atmospheric corrosion galvanic corrosion modeling developed over the years [10-14] to the cases of interest is the assumptions of those of linear or simple Tafel electrochemical boundary conditions. In addition, the models in the literature have no means to include new physical/chemical data without substantial reprogramming.

Although originally developed to study the electrochemical and chemical conditions within crevices, the computational code CREVICER [15] has been extended to study thin electrolyte systems (i.e., atmospheric corrosion) [16-18]. This model framework features an object-oriented design which organizes the program into discrete, independent objects which can be reprogrammed and debugged separately. Through these objects, information is passed into and out of the solving portion of the code. The code can be easily modified to model different materials. Furthermore, the code can handle polarization curves that reflect the pitting-limited passivity exhibited by most corrosion-resistant alloys in natural environments. In this study, CREVICER was extended to study the wetted metal surface coupled to a localized corrosion site.

Due to the extensive literature available on its localized corrosion phenomenology, SS316L was chosen as the material of interest. The total net cathodic current that the wetted metal surface was capable of delivering was selected as the output parameter of interest. This total net cathodic current, I_{net}, is influenced by water layer thickness, size of cathode (*i.e.*, the area of wetted surface), chloride concentration, kinetic parameters (exchange current density $i_{o,c}$ and Tafel slope β_c of the cathodic reaction, anodic passive current density i_p of the wetted surface), and the repassivation potential E_{rp}. The effects of these variables were explored using values that from the literature for SS316L.

The cathodic reaction taking place on wetted metal surfaces of corrosion resistant alloys exposed to ambient atmospheres is expected to be mainly oxygen reduction. The reaction could be under activation, mass or mixed control. The activation portion is described well with a Tafel law. In this study, polarization curves were constructed based on experimental data (reversible potential $E_{o,c}$, exchange current density $i_{o,c}$, and Tafel slope β_c) and theoretical calculations (limiting oxygen reduction current density i_{lim}). The model was also able to include the anodic passive current density (i_p) which has been ignored in models previously reported in the literature.

The goal of this study was to characterize the potential and current distributions of a wetted metal surface coupled to a localized corrosion site, as a means of exploring the effects of various parameters, and quantify the extent to which the rates of localized corrosion can be supported by cathodic reactions within a thin electrolyte. Specifically, dependencies of the I_{net} for the cathode on the kinetic and physiochemical parameters described above were explored.

MODEL DESCRIPTION

The model shown in Figure 1 was used to simulate the atmospheric exposure of a SS 316L substrate covered by a layer of electrolyte thin film and containing a creviced region. As stated earlier, this study investigated only the external wetted surface (circled portion of Figure 1a) portion of the system (shown in Figure 1b). The wetted surface was assumed to have a varying length of Lc and a constant width of 10μm (an arbitrarily-picked value small enough to represent a pseudo 1-D geometry; the choice of this value

has no effect on results). The surfaces were, as illustrated in Figure 1c, simulated with meshes generated by ANSYS®. The concentration of elements, as illustrated in Figure 1c, was highest close to the crevice mouth where the potential/current density gradients were expected to be highest. The electrolyte thin film was assumed to be homogeneous (constant conductivity) and have a constant thickness of WL).

Although the CREVICER code can take into account diffusion, migration and generation of species, it was assumed here that gas/electrolyte transport had reached equilibrium, electrical potential distributions had reached a steady state, and that there existed a stable electrolyte chemistry. Given that the electrolyte conductivity was assumed to be constant, the Laplace equation can be applied:

$$\nabla^2\Phi = 0 \qquad (1)$$

NaCl was assumed to be the only species in the near neutral thin film electrolyte which had a solution conductivity κ,

$$\kappa = \Sigma(z_j \cdot F^2 \cdot \mu_j \cdot C_j) \qquad (2)$$

where z_j is the charge of species j, μ_j is the corresponding mobility, and C_j is the concentration. Ion/ion interactions occurring in concentrated solutions were incorporated into C_j by multiplying the actual C_j with a correction factor smaller than 1 while assuming μ_j is constant. The correction factors were estimated from experimental conductivity data [19]. For example, for a solution with 1M NaCl, this correction factor was ~0.88 and the C_j used to calculate κ thus was 0.88M instead of 1M.

The electrolyte layer was treated as a stagnant layer and the oxygen diffusion coefficient was assumed to be constant. Oxygen solubility data were obtained from data which took into account the effect of salinity [20].

BOUNDARY CONDITIONS

The end of the wetted SS 316L surface coupled to the crevice was held at the latter's repassivation potential E_{rp}, which was estimated to be -0.35V for SS 316L based on data published in literature [21-23]. The wetted surface was further assumed to have a uniform passive current, i_p, and a cathodic current density

$$i_c = \frac{i_{o,c} \cdot e^{\frac{2.3(E-E_{o,c})}{\beta_c}}}{1+\frac{i_{o,c}}{i_{\lim}} \cdot e^{\frac{2.3(E-E_{o,c})}{\beta_c}}} \qquad (3)$$

where $i_{o,c}$ is the exchange current density, and $E_{o,c}$ is the reversible potential for the cathodic reaction respectively, β_c is the Tafel slope; and i_{lim} is the diffusion-limited oxygen reduction current density which can be estimated from

$$i_{\lim} = \frac{nFDC}{WL} \qquad (4)$$

where n (n=4) is the number of charges involved in the oxygen reduction, D is the oxygen diffusion coefficient (assumed to be 10^{-5} cm^2/s), and C is the concentration of dissolved oxygen in electrolyte adjacent to the gas/liquid interface [24].

The net cathodic current density i_{net} for each element can be calculated as

$$i_{net} = i_c - i_p \quad (5)$$

The values of $E_{o,c}$, $i_{o,c}$ and β_c (-0.05V, 10^{-9} A/cm^2, and 0.1 V/dec, respectively) were estimated from the experimental data of SS 316L in simulated seawater reported by Sridhar et al. [23] and served as the inputs of base cases. A passive anodic dissolution current density $i_p = 10^{-8}$ A/cm^2 was assumed. This passive current density, combined with the choice of cathodic polarization parameters, would yield a corrosion potential E_{corr}=-0.15 V for the SS316L surface if the surface were not coupled to an active crevice. This value of E_{corr} roughly approximates that found experimentally [23].

The temperature considered in this study was 25°C. The base cases studied were chosen to bracket a range of water layer thickness (WL), chloride concentration ([Cl^-]) and length of cathode (Lc) of practical importance. A three-level, full factorial design [25] of these three parameters was performed to quantify the effects of these parameters as well as their possible interactions. Table 1 lists the parameter values used.

Table 1. Values of WL, [Cl^-] and Lc used in a full factorial design

WL (μm)	[Cl^-] (M)	Lc (cm)
10; 25 ; 200	0.001; 0.05; 1	0.25; 1 ; 10

Table 2 lists all of the input values of kinetic parameters used in the base cases; note that i_{lim} is a function of the dissolved oxygen concentration which decreases with increase of salinity ([Cl^-]) [26,27] and water layer thickness (WL). Figure 2 shows the schematic of electrode kinetics used: the oxygen reduction reaction (i_c, dashed line) in an electrolyte film with WL=10μm and [Cl^-]=0.001M; the passive behavior of the stainless steel (i_p, solid vertical line) and the summation of the two (i_c-i_p) (thick solid line, which overlaps with i_c at potentials well below E_{corr}). When the WL increases, as shown in Figure 2 as

well, the limiting current density decreases significantly. However, as highlighted by the shaded zone, the SS 316L is apparently under activation control in the range of potentials of interest of this study.

Table 2. Values of Kinetic Parameters used in base cases

$E_{o,c}$ V	E_{rp} V	E_{cor} V	i_p A/cm^2	$i_{o,c}$ A/cm^2	i_{lim} A/cm^2	β_c V/dec
-0.05	-0.35	-0.15	10^{-8}	10^{-9}	$\frac{4FDC}{WL}$	0.1

The effects of E_{rp}, i_p, $i_{o,c}$, and β_c were studied by performing full factorial designs of Lc and [Cl^-] shown in Table 3. To save calculation time, however, only WL=25μm was considered, and yet the number of calculations still amounted to 90 (=10 x 9).

Table 3. Values of parameters used to exam their effect on the galvanic coupling

E_{rp} (V)	i_p (A/cm^2)	$i_{o,c}$ (A/cm^2)	β_c (V/dec)
-0.25, -0.35, -0.45	10^{-8}, 10^{-9}	10^{-9}, 10^{-10}	0.1, 0.13, 0.16

* For each parameter, full factorial design of Lc and [Cl^-] was used while WL was fixed at 25 μm

The governing equation with the boundary conditions of interest was solved using a FEM approach [15], and outputs of the code were E(x) and i(x). The net cathodic current density i_{net} on each element was calculated within the code by subtracting i_p from the i_c corresponding to the average E of the element, and a total net cathodic current I_{net} was calculated by integrating net cathodic current for all of the elements. The magnitude of I_{net} was used to quantitatively compare the effects of individual parameters on the ability of the thin-electrolyte cathode to support a localized corrosion site.

RESULTS

1. Typical Current and Potential Distribution

Figure 3 shows typical potential and corresponding net current density distributions calculated from the model. The potential of cathode increased away from E_{rp} towards the E_{corr} of the cathode, as the distance from the crevice increased, as expected. Simultaneously, the corresponding net cathodic current i_{net} decreased with increasing distance from the crevice. Figure 3 also supports the assumption used in the selection of the meshing that the potential/i_{net} gradients are the highest at elements adjacent to localized corrosion site. Moreover, the figure indicates that the chloride concentration has a significant effect on the potential/current distributions.

2. Base Cases

Figure 4 illustrates the main effect of each parameter. Each data point corresponds to the summation of nine cases (the full factorial design of the other two parameters and three levels other than the fixed parameter). All three parameters (WL, Lc and [Cl^-]) have significant impact on I_{net}; higher WL, Lc, or [Cl^-], within the testing range, resulted in higher I_{net}.

Figure 5 suggests considerable interactions between Lc and [Cl^-], Lc and WL. For example, as shown in Figure 5a, when [Cl^-] was 0.001M, the effect of increasing Lc was negligible as I_{net} remained essentially constant; however, when [Cl^-] was 1M, I_{net} increased from 2.5×10^{-10} to 4.2×10^{-9} A when Lc increased from 0.25 cm to 10cm.

3. Effects of kinetic parameters ($i_{o,c}$, i_p, E_{rp}, β_c)

The $i_{o,c}$ was found to have significant effect on total net cathodic current I_{net}. The ratio $R_c=I_{net}(i_{o,c}=10^{-9})/I_{net}(i_{o,c}=10^{-10})$ was used to quantify the effect. As shown in Figure 6, increasing $i_{o,c}$ by a factor of 10 resulted in an increase of I_{net} by a factor between 4 and 11. Figure 6 also suggests that [Cl^-] and Lc both have some interaction with $i_{o,c}$ within the range of interest. Cases with higher [Cl^-] (or smaller Lc) typically had higher R_c; for example, for a case with 1cm cathode and 1M chloride, the ratio R_c was ~11, whereas this ratio decreased to ~4 for the same size cathode with only 0.001M chloride. Despite the large variation observed with [Cl^-] at smaller Lc, R_c tends to approach a constant value (~4) as Lc increases to a value large enough so that I_{net} saturates.

Similar to the study of $i_{o,c}$ effect, the effect of i_p (10^{-9} and 10^{-8} A/cm^2) was quantified using the ratio $R_a=I_{net}(i_p=10^{-9})/I_{net}(i_p=10^{-8})$. Figure 7 shows that the change of i_p by a factor of 10 results in little difference in I_{net}, regardless of the choices of cathode size Lc and chloride concentration [Cl^-].

E_{rp} was found to have significant impact on the I_{net}. To quantify the effect of E_{rp}, the ratio $R_{Erp}=I_{net}(E_{rp}$=-0.35 or -0.45V)/$I_{net}(E_{rp}$=-0.25V) was used. As shown in Figures 8a and 8b, decreasing E_{rp} from -0.25V to -0.35V resulted in a R_{Erp} between 3.8 and 11. When E_{rp} was further decreased to -0.45V, R_{Erp} increased to a value between 12 and 103. The figures also show that R_{Erp} decrease with increase of Lc. Despite its large variation with [Cl^-] at smaller Lc, R_{Erp} tends to approach to a constant value (~4 for E_{rp}=-0.35V, and ~12 for E_{rp}=-0.45V) as Lc increases.

The effect of the cathodic reaction Tafel slope β_c was quantified with the ratio $R_{\beta c}=I_{net}(\beta_c$ =0.13 or 0.16V)/$I_{net}(\beta_c$ =0.1V). Figure 9a and 9b show that β_c has significant

effect on I_{net}. Increasing β_c from 0.1 to 0.13 V/dec resulted in a $R_{\beta c}$ between 0.2 and 0.47; and it further decreased to a value between 0.07 and 0.27 when β_c was 0.16 V/dec. Figure 9 also show that $R_{\beta c}$ increases with increasing Lc and [Cl^-]. Apparently Lc and [Cl^-] have significant impacts on the effect of β_c. Moreover, like E_{rp}, the importance of β_c is greatest at low Lc, and the effect appears to be disappearing at large Lc as I_{net} approaches saturation.

DISCUSSION

For corrosion resistant materials exposed to ambient atmospheric environments, the corrosion mode of highest risk is expected to be localized corrosion (pitting, crevice, stress-corrosion cracking). However, most atmospheric corrosion research has focused mainly on the more uniform corrosion exhibited by Ni and Cu when exposed to atmospheres of differing relative humidity, temperature, and gaseous pollutant type and concentration [28-32].

Fundamental study of localized corrosion in thin electrolytes has been limited. Whether or not localized corrosion in a thin electrolyte can cast a threat to **structural** integrity depends on the ability of the localized corrosion site to stabilize. Stabilization of localized corrosion requires that the site must dissolve at a sufficiently high rate as to maintain the high local metal ion concentration (and therefore the chloride ion concentration) against diffusion. In addition, the degree to which an anodic site can interact with the surrounding cathodic areas will affect the maximum rate of localized corrosion in conjunction with the kinetics within the localized corrosion site. Under

freely corroding conditions, stabilization requires ionic and electrical connection between the localized corrosion sites and a sufficiently robust cathodic area [6,7]. The robustness of the cathodic area depends in large part on the chemistry, electrochemistry, and, under atmospheric conditions, the geometry of the thin electrolyte. A systematic study of all these parameters and their interactions is more tractable computationally than experimentally. Although the effects of the electrochemical parameters may be qualitatively estimated based on Mixed Potential Theory, the intervening distributed electrolyte resistance and subsequent potential drop prevents quantitative evaluation using analytic solutions except in cases of very simple interfacial kinetics. Numerical computational studies allow quantitative investigation of these parameters.

The objective of this study was to characterize the ability of cathodes exposed to thin-film electrolytes to support a stable localized corrosion site, to explore the effects of thin film chemistry, geometry, and electrochemistry, and to contribute to the establishment of a scientific basis for the prediction of the stabilization of localized attack on wetted, corrosion resistant material surface.

1. Effects of WL, Lc, and [Cl^-]

In describing atmospheric corrosion, the two parameters that are most often cited are the water layer thickness and the environment composition. In this work, a range of WL was investigated to determine the relative importance of those variations to changes in other parameters. The environment composition was varied by changing the [Cl^-]. The primary direct effect of [Cl^-] was the change in the solution conductivity, although the effects on oxygen solubility were also included. It should be noted that although E_{rp} can

depend on the chloride concentration, that effect was not directly accounted for in this work. Nonetheless, the effect of varying E_{rp} was investigated separately (Figure 8). The ability to separate out such effects is one of the advantages of computational modeling.

Table 4. Analysis of Variance for the full factorial design of WL, Lc, and [Cl^-]

Source of variance	WL	Lc	[Cl^-]	WLxLc	WLx[Cl^-]	Lcx[Cl^-]	WLxLcx[Cl^-]
Ratio to WL	**1**	**5.19**	**3.85**	**0.74**	0.18	**2.46**	0.24

A standard analysis of variance [25] was performed on the full factorial design of WL, Lc and [Cl^-], and the sum of squares was normalized with respect to the sum of square of WL. Table 4 lists results of the analysis, showing that WL, Lc, [Cl^-] as well as interactions of WL x Lc, and Lc x [Cl^-] are of significance. The effects of interactions of WL x [Cl^-] and WL x Lc x [Cl^-] were very small. Based on the magnitude of normalized sum square listed in Table 4, the effects of these five parameters follows the ranking: Lc>[Cl^-]> Lc x [Cl^-] >WL> WL x Lc. Note that the interaction between Lc and [Cl^-], (Lc x [Cl^-]), had a larger effect than did WL alone. Thus, the three most important effects do not involve WL, which is generally considered to be a primary factor. This is likely because the SS 316L is under activation control in the range of potentials of interest and change in WL consequently has little effect on the corresponding cathodic reaction.

The data were also fitted using linear regression for two cases. In one case, only three factors (WL, Lc, and [Cl^-]) were used; whereas in the second case, all five of the factors found to be significant were included.

The three-factor regression was found to be

$$I_{net} = 4.37 \cdot 10^{-12} \cdot WL + 1.55 \cdot 10^{-9} \cdot [Cl^-] + 1.95 \cdot 10^{-10} \cdot Lc - 5.9 \cdot 10^{-10}$$

$$R^2=0.42 \qquad (6)$$

The five-factor regression was found to be

$$I_{net} = -1.36 \cdot 10^{-13} \cdot WL + 2.46 \cdot 10^{-11} \cdot [Cl^-] - 4.14 \cdot 10^{-11} \cdot Lc + 1.20 \cdot 10^{-12} \cdot WL \cdot Lc$$

$$+ 4.07 \cdot 10^{-10} \cdot [Cl^-] \cdot Lc + 2.95 \cdot 10^{-10} \qquad R^2=0.88 \qquad (7)$$

where the units are μm for WL, M for [Cl^-] and cm for Lc.

These two functions were used to estimate I_{net} of the full factorial design. The corresponding results are presented in Figure 10 and compared to the model computation data. The figure shows that the 5-factor regression (R^2=0.88) is, as would expected, better than the 3-factors regression (R^2=0.42).

As discussed below, the I_{net} actually saturates when Lc increases above a certain value that depends on the values of WL, [Cl^-], and the kinetic parameters. Therefore, the regression can only serve as a tool of rough estimation of I_{net} within the parameter limits of the full factorial design (i.e., 10μm<WL<200μm, 0.001M<[Cl^-]<1M, and 0.25cm<Lc<10cm). This saturation effect is one of the reasons that neither simple Mixed Potential Theory estimates nor non-dimensionalized variables can capture the behavior of localized corrosion stabilization in thin electrolytes. Numerical evaluations are required.

2. Effects of kinetic parameters ($i_{o,c}$, i_p, E_{rp}, β_c)

The polarization behavior of electrochemical processes as well as the repassivation potential of a material such as SS 316L vary with many factors such as temperature, exposure time, solution chemistry, surface condition, etc [33,34]. Thus, it is almost impossible to use one set values of $i_{o,c}$, i_p, E_{rp} and β_c to represent actual behavior of the studied system. A plausible approach to overcome this challenge is to parameterize these

parameters to envelope possible experimental values. With careful design, the computational experimental process can also quantify the effect of each parameter and thus identify parameter(s) of importance.

For example, it is expected that lower $i_{o,c}$ will result in lower I_{net} because decreasing $i_{o,c}$ (provided $E_{o,c}$ and β_c remain constant) will consequently decrease the capacity of the cathode to provide current at any fixed potential. Cui [34] indeed reported that the cathodic polarization curves of sandblasted SS 316L rebar shifted to lower current densities as the exposure time increase, suggesting a decrease in $i_{o,c}$ with time. The total projected I_{net} would accordingly decrease with time, leading to greater instability for the localized corrosion system, eventually leading to repassivation if I_{net} becomes low enough. Issues of this kind are far more tractable computationally than experimentally.

A simple way to check the effect of i_p is to compare i_p with i_c at E_{rp} (which drives the cathode). With an E_{rp}=-0.35V, $i_{o,c}=10^{-9}$A/cm^2, and β_c=0.1V/dec, i_c at -0.35V is 10^{-6}A/cm^2. Thus, a change of i_p from 10^{-8} to 10^{-9} A/cm^2 (as might occur from improved passivity with time) would result in little change (from $0.99\cdot10^{-6}$ to $0.999\cdot10^{-6}$A/cm^2) in i_{net} at this potential. Therefore, it was anticipated that this change of i_p will have negligible effect on I_{net}. This reasoning was confirmed by computation analysis shown in Figure 7. For all the cases studied, changing i_p had no effect, with the ratio of the I_{net} of two i_p being 1.013±0.006. This is not the case, however, if i_p is not trivial compare to i_c (at E_{rp}), as it might be if an active nose is present that is only somewhat smaller than i_c at E_{rp}.

With all the other kinetic parameters fixed, increasing E_{rp} decreases I_{net}. Computation showed that an increase of 0.2 V in E_{rp} (from -0.45 to -0.25V) decreased I_{net} ~12-100 times depending on [Cl^-] and Lc. The reason for this significant effect of E_{rp} is clear; less

overpotential for the cathodic reaction leads to lower currents when the cathodic reaction is activation controlled. This effect also contributes to the observation that a lower E_{rp} for a material leads to more severe localized corrosion attack. In natural exposures, it is the external cathode that supplies the cathodic current, not a potentiostat as in most laboratory studies. Lower E_{rp} results in cathodes being able to supply more current. Limitations on the cathode thus lead to a high sensitivity of localized corrosion to the raising E_{rp}.

The effect of β_c was found to be important as well. Whereas a Tafel slope of β_c=0.1V/dec was estimated from the data reported by Sridhar et al [23], effective Tafel slopes vary in natural systems. Accordingly, based on this study, I_{net} could vary significantly; the larger β_c, the smaller I_{net}, provided other parameters remain constant.

The effects of the interfacial kinetic parameters can also be qualitatively analyzed by using the E-log i plot illustrated in Figure 2 and applying Mixed Potential Theory. For example, increasing $i_{o,c}$ will shift the i_{net} curve to the right. Given an E_{rp} fixed at -0.35V, this change suggests a significant increase in I_{net}. Changing the Tafel slope βc from 0.1 to 0.16 essentially rotates the E-log i curve in Figure 2 clockwise, indicating a decrease in I_{net}. Although this analysis can qualitatively project the direction of the effects, it can not give quantitative estimation of the actual effects because of the intervening distributed resistance of the electrolyte, particularly at large Lc.

While the effects of these parameters were complicated by their intrinsic dimensional difference and interaction with Lc and [Cl^-], as suggested by Figures 6-9, the R ratios all appear to approach limiting values R_{lim} with Lc. Using R_{lim} as criteria, the effects of these parameters decreased in the following order: $E_{rp}>i_{o,c}>b_c,>>i_p$.

3. Saturation of Total Net Cathodic Current I_{net}

Figures 5a and 5b show that I_{net} tends to saturate when Lc exceeds a critical value. The origin for I_{net} saturation is the increase in the potential of the interface with increasing distance to the anode, and the corresponding substantial decrease in the net cathodic current density, i_{net}. Although the Tafel behavior dominates this effect, the inclusion of i_p in the representation of the boundary conditions is of substantial importance. The ignoring of the presence of i_p would either lead to an overestimate of the total cathodic current available for systems that reach the E_{corr} of the cathode (due to the ignoring of the use of some of that current to balance i_p at E_{corr}), or would result in the calculation of non-physical potential profiles (*i.e.*, the potential at positions of the cathode far away from the anode would rise above the E_{corr} of the cathode).

In many cases, I_{net} shown did not reach saturation at Lc=10cm. Computation on other sizes of cathodes (4, 15, 20 and 30cm) were performed to determine the saturation limit for different cases. Figure 11a plots I_{net} as a function of Lc for the cases with a constant WL of 25μm and three levels of $[Cl^-]$ (0.001, 0.05, and 1M). It shows that the I_{net} saturation limit (hereafter referred to as I_{max}) and the Lc at which it is observed significantly increases with $[Cl^-]$. For example, I_{max} was reached when Lc was as small as 1cm for a case with 0.001M chloride, whereas I_{max} was only reached when Lc was 30cm for a case with 1M chloride. Computations on cases with fixed WL=10 or 200 μm were performed as well and showed similar saturation behavior of I_{net}.

Figure 11b illustrates similar I_{net} saturation behavior while highlighting the effect of WL. The cases shown all have a constant $[Cl^-]$ of 1M. Cases with 0.001M or 0.05M $[Cl^-]$

were also studied and the results showed similar saturation behavior of I_{net} and effect of WL.

4. Impact of Cathodic Limitations on Localized Corrosion Stability

The smallest size of cathode at which I_{max} is realized and the magnitude of I_{max} are of practical importance in the determination of the stability of localized corrosion in thin film electrolytes under natural conditions. In most cases, thin electrolytes are not contiguous over an entire structure, but instead form patches of electrolyte. The question of importance is what size patch of electrolyte could stabilize a localized corrosion site.

Because I_{max} is approached asymptotically, 98% I_{max} was used to compare required minimum Lc for current saturation. Table 5 lists the Lc needed to reach 98% I_{max}. This type of table can be of practical use in two ways. First, it allows the determination of limiting size of cathode beyond which no significant extra current (<2%) can be supplied by the cathode. This approach to calculation allows experimentalists to design exposure specimens that offer limiting behavior for a given set of corrosion conditions.

In addition, this approach allows a link to be made to the stability of localized corrosion sites. Minimum localized corrosion site dissolution rates have been determined both theoretically and experimentally. Galvele [35] proposed that, for a pit to remain stable, the parameter $x \cdot i$ (where x is the depth of the site, and i is the current density at the base of the pit) must exceed a critical value determined by the hydrolysis reactions of the metal involved and the dependence of the anodic kinetics in the pit on pH. Such an approach has been validated by Newman [36] and Scully [37]. Thus, given the size and minimum current density i of a localized corrosion site, the minimum current required to

stabilize the site can be calculated. This current must be supplied by the cathode in a natural system. The ability for a given cathode to provide such a current is described by I_{net}. Thus, these calculations allow the determination of the stability of localized corrosion couples involving finite-sized cathodes covered with thin electrolytes.

Table 5 Computation projected Saturation limit

WL μm	10			25			200		
$[Cl^-]$ M	0.001	0.05	1	0.001	0.05	1	0.001	0.05	1
Lc (cm) needed for 98% I_{max}	1	4	15	1	10	30	4	15	30+
98% I_{max} **(10^{-8}A)**	**0.01**	**0.07**	**0.29**	**0.02**	**0.11**	**0.47**	**0.04**	**0.31**	**>1.2**

* Choice of kinetic parameters is listed in Table 2.

CONCLUSIONS

The ability of cathodes (e.g. wetted SS316L surface) exposed to thin electrolytes to support a stable localized corrosion site was studied computationally because the distributed resistance between the localized corrosion site and positions on the wetted cathode and the nonlinear interfacial kinetics make accurate estimates of the effects of important variables using simple Mixed Potential Theory or nondimensionalization methods only qualitative. The effect of relevant physical and electrochemical parameters on the total net cathodic current I_{net} was explored. The following conclusions can be drawn:

1. All three main parameters, WL, Lc and $[Cl^-]$, as well as the interactions of Lc and WL, and Lc and $[Cl^-]$ have significant impact on total net cathodic current I_{net} that the wetted surface can supply to support localized corrosion. Analysis of Variance

showed that the effects of these factors decrease in the following order: Lc>[Cl^-]> Lc x [Cl^-]> WL > WL x Lc. Note that the three most important effects do not involve WL, a non-intuitive observation.

2. Linear regression gave only a fair estimation of the computation results (R^2=0.88), demonstrating that simple scaling laws cannot be applied to predicting stability of localized corrosion in thin electrolyte films.
3. Cathodic kinetic parameters, E_{rp}, $i_{o,c}$, and β_c, were found to have significant effects on I_{net} following the order $E_{rp}>i_{o,c}>\beta_c$, whereas i_p in the cases of studied had little effect on I_{net}. Mixed Potential theory can estimate the effect of these parameters graphically, but only qualitatively, due to the importance of the distributed resistance of the thin electrolyte layer.
4. The total net cathodic current I_{net} was found to reach limiting values (I_{max}) as the cathode size Lc increased. The 98% I_{max} (used instead of I_{max} because I_{net} typically gets saturated very slowly) as well as the corresponding characteristic Lc of cases with various WL and [Cl^-] (each three 3 levels) were determined.
5. The projected 98% I_{max} may be used to estimate the stability of a localized corrosion site coupled to wetted cathodic surface, and the corresponding Lc provides important information of experimental design and corrosion protection.

Acknowledgements

This work was supported by the Office of Science and Technology International of the United States Department of Energy (DOE) and carried out as part of the DOE Multi-University Corrosion Cooperative under Cooperative Agreement DE-FC28-04RW12252.The funding agency is gratefully acknowledged.

References

[1] C. Leygraf, T.E. Graedel, Atmospheric Corrosion The Electrochemical Society, Penington, NJ 2000, p. 9

[2] R.P. Wayne, Chemistry of Atmosphere, 3rd Edition, Oxford University Press, Oxford, UK 2000, p. 83

[3] Z. Szklarska-Smialowska, Pitting Corrosion of Metals, National Association of Corrosion Engineers, Huston, TX 1986, p. 3

[4] G.S. Frankel, J. Electrochem. Soc. 145 (1998) 2186

[5] R.G. Kelly, Crevice Corrosion, In: M. Stratmann, G. S. Frankel (Eds), Encyclopedia of Electrochemistry, 2003 WILEY-VCH Verlag GmbH & Co. KGaA, Weinheim, Germany, 2003, Vol. 4, p. 275

[6] H.W. Pickering, Corrosion, 42(1986) 125

[7] Z. Szklarska-Smialowska, Pitting Corrosion of Metals, National Association of Corrosion Engineers, Huston, TX 1986, p. 43

[8] N.G.Thompson, B.C. Syrett, Corrosion, 48 (1992) 649

[9] N. Sridhar, G.A. Cragnolino, Corrosion, 49(1993) 885

[10] E. McCafferty, J. Electrochem. Soc. 124 (1977) 1896

[11] P. Doig, P.E.J. Flewitt, Philosophical Magazine B, 38 (1978) 27

[12] P. Doig, P.E.J. Flewitt, J. Electrochem. Soc. 126 (1979) 2057

[13] R. Morris, W. Smyrl, J. Electrochem. Soc. 135 (1988) 723

[14] R. Morris, W. Smyrl, J. Electrochem. Soc. 136 (1989) 3229

[15] K.C. Stewart, Ph.D. Dissertation, University of Virginia, 1999

[16] F. Presuel-Moreno, F. Cui, R.G. Kelly, Modeling of Corrosion Protection Provided by an Aluminum-Based Clad: Water Layer Effect, in: R. G. Buchheit, R. G. Kelly, N. A. Missert, B. A. Shaw, (Eds), Corrosion and Protection of Light Metal Alloys, PV 2003-23, p. 344, The Electrochemical Society, Inc., Pennington, NJ (2004)

[17] H. Wang, F. Presuel, R. G. Kelly, Electrochimica Acta, 49(2), 239 (2004)

[18] F. Cui, F. Presuel-Moreno, R.G. Kelly, "Experimental And Computational Evaluation Of The Corrosion Of Alclad AA2024-T3 Exposed At A Seacoast Environment," in: D.A. Shifler, P.M. Natishan, T. Tsuru, S. Ito, (Eds.), F2-Corrosion In Marine And Saltwater Envirionment II, PV2005-14, The Electrochemical Society, Inc., Pennington, NJ (2005), pp. 201-216

[19] R.S. Carmichael Editor, CRC Handbook of Physical Properties of Rocks, Volume 1, CRC Press, Inc., Boca Raton, FL 1982, p. 273

[20] http://www.colby.edu/cpse/equipment2/simple/algo.html

[21] D.S. Dunn, G.A. Cragnolino, N. Sridhar, Corrosion, 56 (2000) 90

[22] A. Anderko, N. Sridhar, D.S. Dunn, Corrosion Sci. 46 (2004) 1583

[23] N. Sridhar, C.S. Brossia, D.S. Dunn, A. Anderko, Corrosion, 60 (2004) 915

[24] E. Gileadi, Electrode Kinetics for Chemists, Chemical Engineers, and Material Scientists, VCH Publishers, Inc, New York, NY 1993, p. 86

[25] D.C. Montgomery, Design and Analysis of Experiments, 4th Edition, John Wiley & Sons, Inc. New York, NY 1997, p.441

[26] S.D. Cramer, Industrial & Engineering Chemistry Process Design and Development, 23 (1983) 618

[27] M. Franchini, H. Unvala, J.T. Carstensen, Journal of Pharmaceutical Sciences, 82 (1993) 550

[28] M. Benarie, F.L. Lipfert, Atmos. Environ., 20 (1986) 1947

[29] T.E. Graedel, J. Electrochem. Soc., 136 (1989) 193C

[30] J.-E. Svensson, L.-G. Johansson, Corrosion Sci., 34 (1993) 721

[31] D. Persson, C. Leygraf, J. Electrochem. Soc., 142 (1995) 1459

[32] J.-E. Svensson, L.-G. Johansson, Corrosion Sci., 38 (1996) 2225

[33] L. Bertolini, M. Gastaldi, M. Pedeferri, P. Pedeferri, and T. Pastore, "Effects of Galvanic Coupling between Carbon Steel and Stainless Steel Reinforcement in Concrete," in: Proceedings of International Conference on Corrosion and Rehabilitation of Reinforced Concrete Structures, 1998, Federal Highway Administration Publication No. FHWA-SA-99-014, FHWA, Mclean, Virginia

[34] F. Cui, Ph.D. Dissertation, University of South Florida, 2003

[35] J.R. Galvele, J. Electrochem. Soc., 123 (1976) 464

[36] R.C. Newman, M. Ajjawi, H. Ezuber, Corrosion Sci., 28 (1988) 471

[37] S. T. Pride, J.R. Scully, J.L. Hudson, J. Electrochem. Soc., 141 (1994) 3028

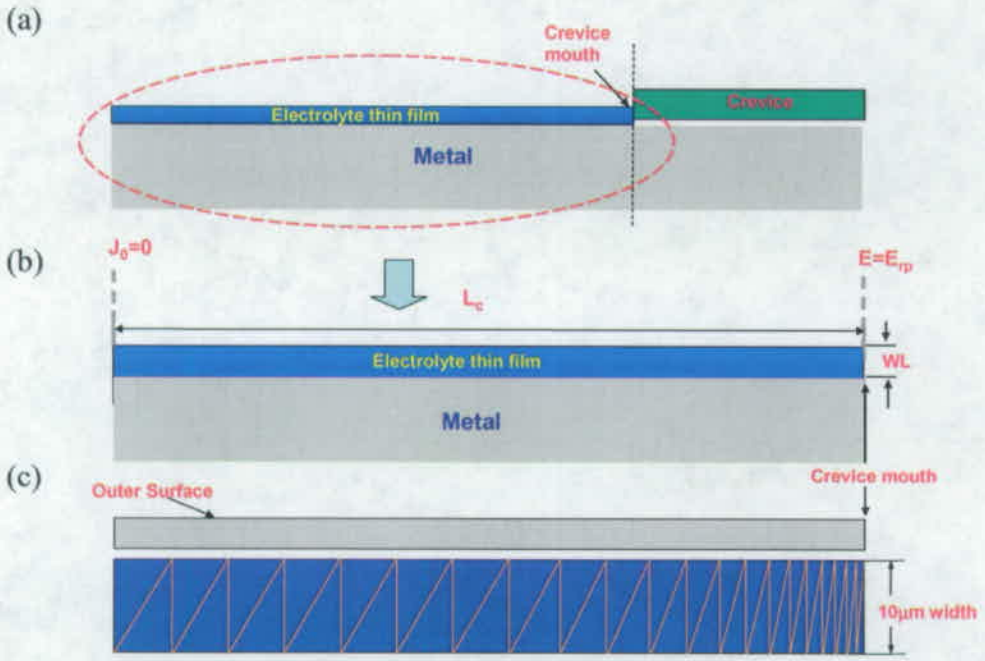

Figure 1. Schematic of the system modeled: a) a typical crevice corrosion system for atmospheric exposure; b) the separated cathode modeled in this paper, where WL is water layer thickness and Lc is the length of the cathode, and it was assumed that the flux at the end of the cathode was 0 (J_o=0); and c) mesh used to represent the cathode surface.

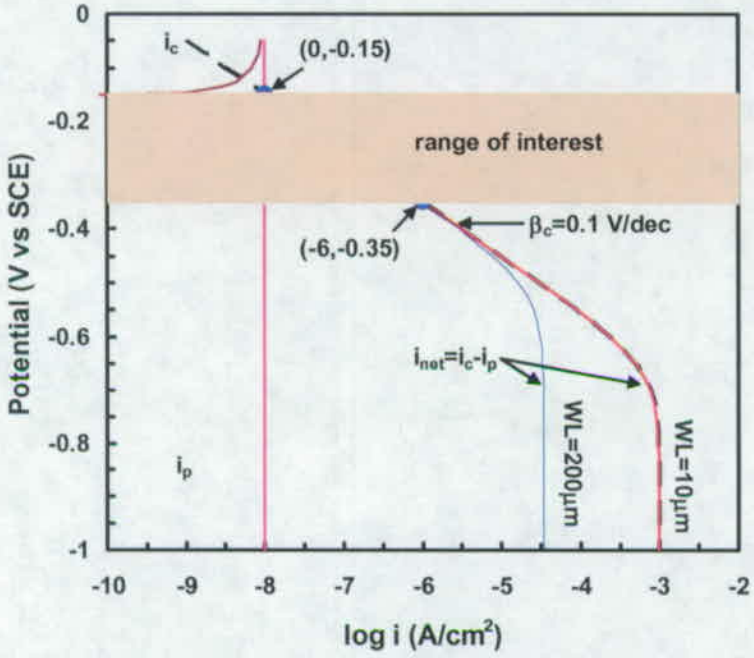

Figure 2. Schematic of cathodic and anodic polarization curves used in base cases. The cathodic process was assumed to have an $E_{o,c}$ of -0.05V (vs SCE), an $i_{o,c}$ of 10^{-9} A/cm^2, and a Tafel slope of 0.1V/dec; the anodic passive current density i_p was assumed to be 10^{-8} A/cm^2. The limiting current density of oxygen reduction i_{lim} decreased with WL and [Cl$^-$]. [Cl$^-$]=0.001M was used in this chart to calculate i_{lim}. In the range of interest, defined by open circuit potential E_{cor} (-0.15V, where i_{net}=0) and repassivation potential E_{rp} (-0.35V, where $i_{net}=10^{-6}$A/cm^2), oxygen reduction was found to be under activation control.

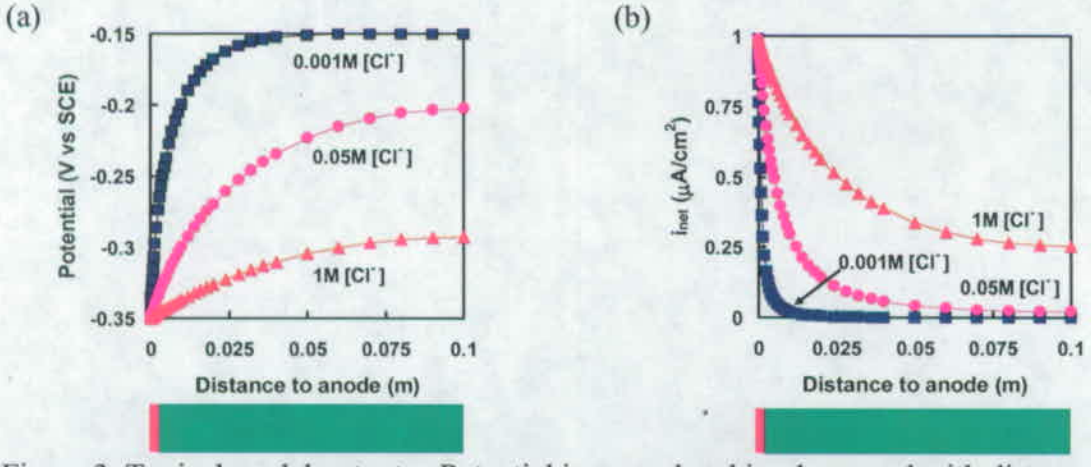

Figure 3. Typical model outputs. Potential increased and i_{net} decreased with distance to anode. Elements near to the anode had the highest potential/i_{net}, and [Cl$^-$] apparently had significant impact on the potential/current density distribution. (Base cases, WL=25 μm, Lc=10cm)

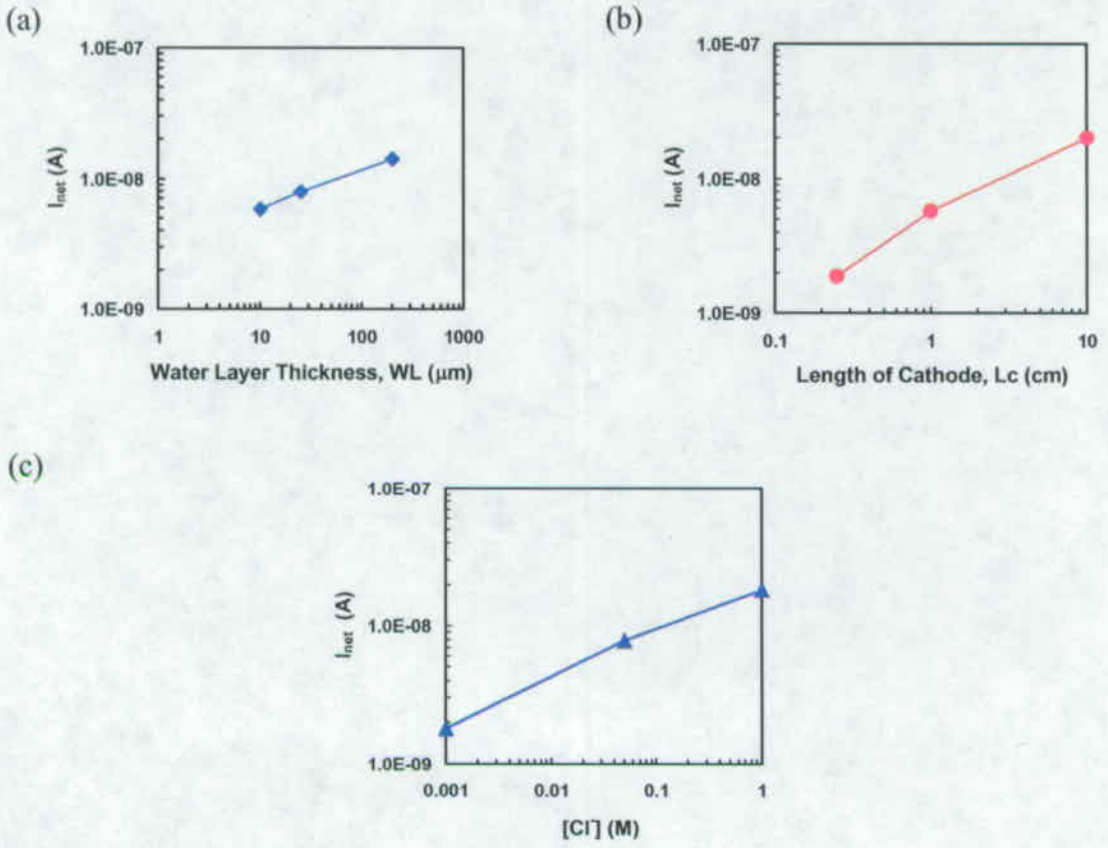

Figure 4. Main effect of WL, Lc and [Cl^-] on I_{net} estimated from the full factorial design analysis of WL, Lc, and [Cl^-]. Each data point in the figures corresponds to the summation of nine cases.

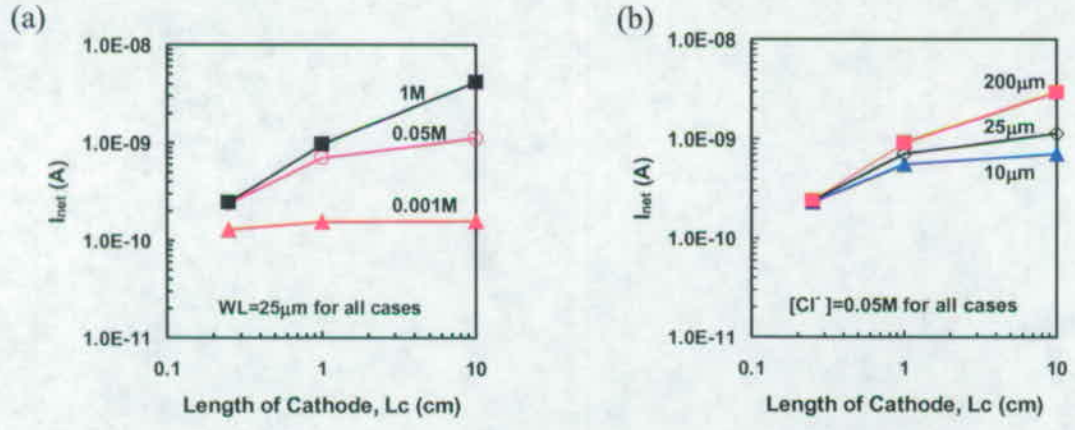

Figure 5. Interaction between parameters: a) effect of length of cathode varies with [Cl^-]; b) effect of length of cathode varies with WL.

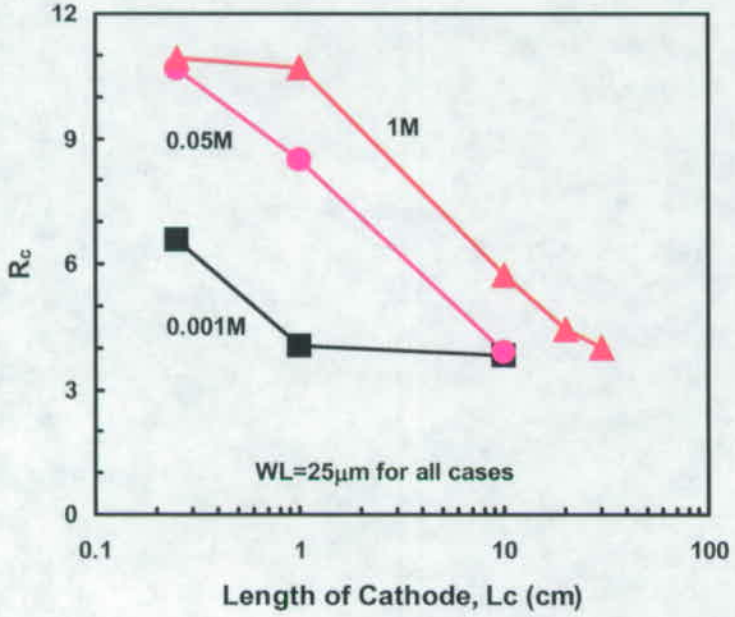

Figure 6. Effect of cathodic exchange current density $i_{o,c}$, as described by $R_c = I_{net}(i_{o,c}=10^{-9})/I_{net}(i_{o,c}=10^{-10})$. Regardless of $[Cl^-]$, R_c tends to asymptote to ~4 at large Lc.

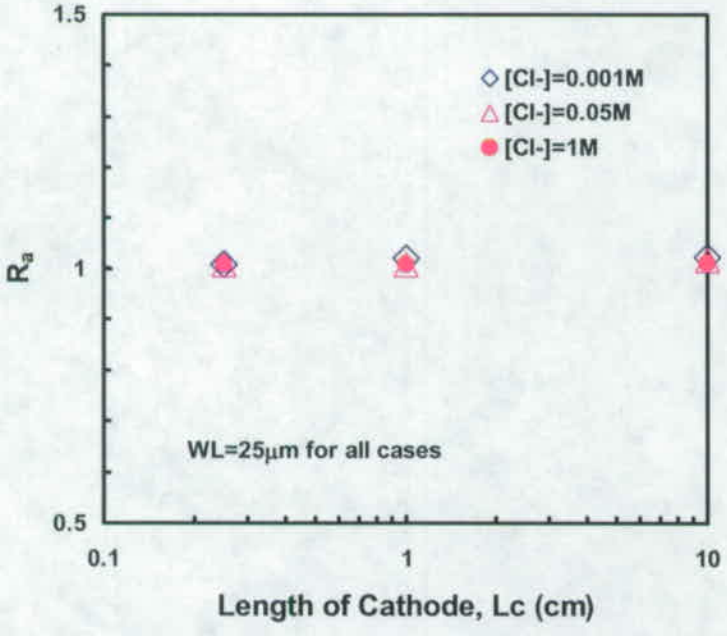

Figure 7. Effect of passive current density i_p, as described by $R_a = I_{net}(i_p=10^{-9})/I_{net}(i_p=10^{-8})$. R_a was 1.013±0.0056 for all cases regardless of values of Lc and $[Cl^-]$.

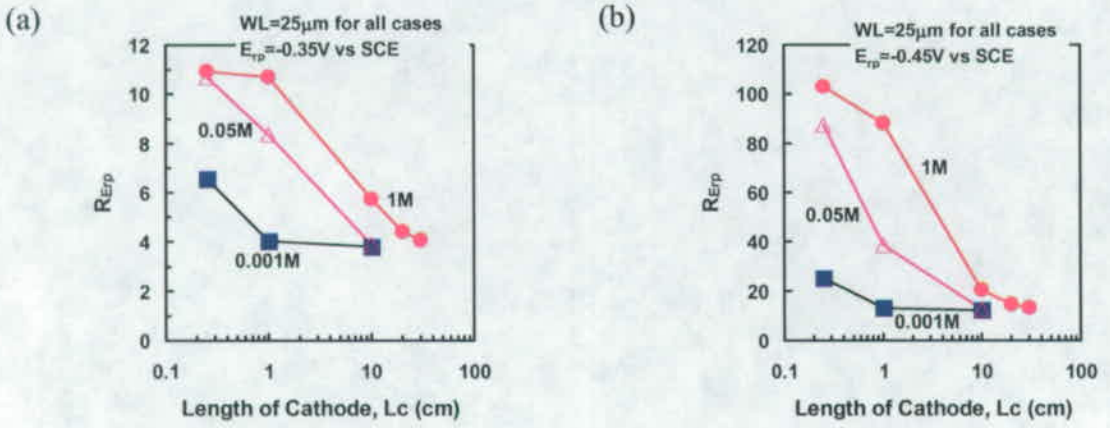

Figure 8. Effect of E_{rp}, as described by $R_{Erp}=I_{net}(E_{rp}=-0.35 \text{ or } -0.45V)/I_{net}(E_{rp}=-0.25V)$: a) $E_{rp}=-0.35$ V; b) $E_{rp}=-0.45$ V. Regardless of $[Cl^-]$, R_{Erp} tends to asymptote to ~4 ($E_{rp}=-0.35V$) and ~12 ($E_{rp}=-0.45V$) respectively at large Lc.

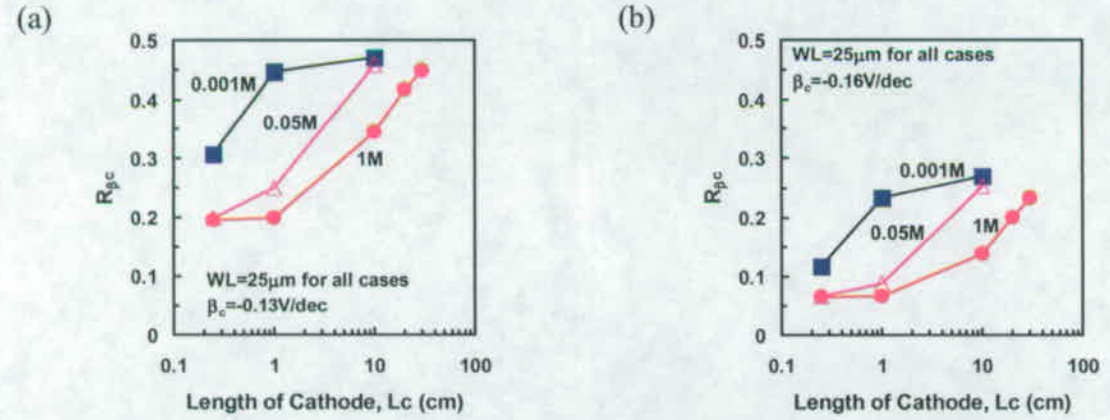

Figure 9. Effect of β_c, as described by $R_{\beta c}=I_{net}(\beta_c=0.13 \text{ or } 0.16V)/I_{net}(\beta_c=0.1V)$: a) $\beta c=0.13$ V/dec; b) $\beta c=0.16$ V/dec. Regardless of $[Cl^-]$, R_c tends to asymptote to ~0.45 ($\beta c=0.13$ V/dec) and ~0.25 ($\beta c=0.16$ V/dec) respectively at large Lc.

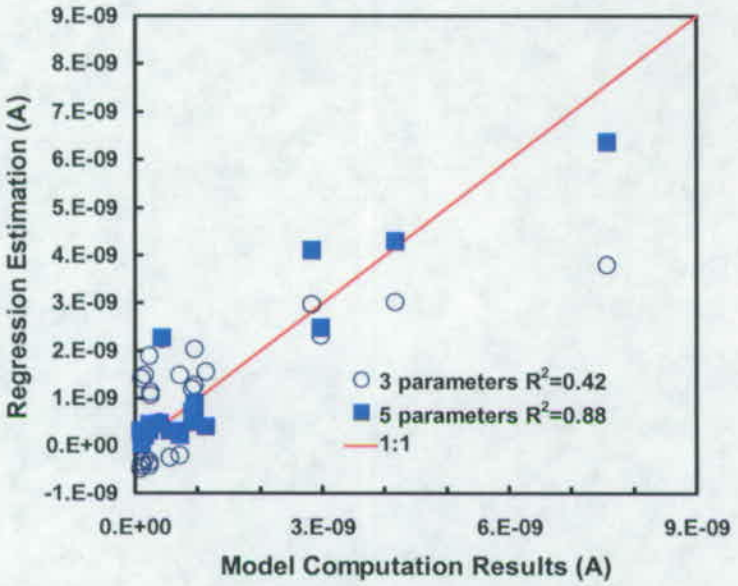

Figure 10. Regression fitting of the computation data using three main factors (WL, Lc, and [Cl^-]) and 5 factors (WL, Lc, [Cl^-], WL x Lc, Lc x [Cl^-]): 5 factors fitting gave better correlation with respect to model data.

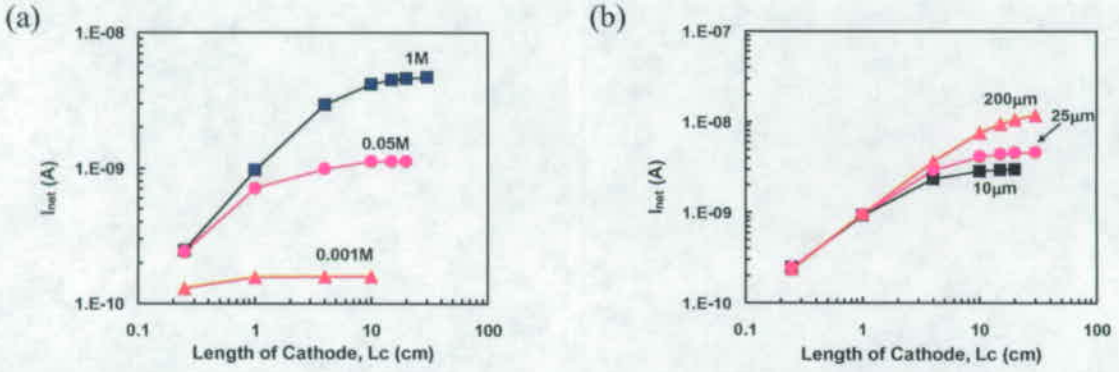

Figure 11. Total net cathodic current I_{net} got saturated as length of cathode increased to a critical value. The speed of saturation depends highly on [Cl^-] and slightly on WL: a) all cases had a constant WL of 25μm; b) all cases had a constant [Cl^-] of 1M, values kinetic parameters are the same as those used in the base cases.